In Situ Synchrotron X-ray Fluorescence Mapping and Speciation of CeO_2 and ZnO Nanoparticles in Soil Cultivated Soybean (Glycine max)

Jose A. Hernandez-Viezcas,[†,§] Hiram Castillo-Michel,[∥] Joy Cooke Andrews,[⊥] Marine Cotte,[∥] Cyren Rico,[†,§] Jose R. Peralta-Videa,[†,§] Yuan Ge,[§,¶] John H. Priester,[§,¶] Patricia Ann Holden,[§,¶] and Jorge L. Gardea-Torresdey[†,‡,§,*]

[†]Chemistry Department and [‡]Environmental Science and Engineering Ph.D. Program, The University of Texas at El Paso, El Paso, Texas 79968, United States, [§]University of California Center for Environmental Implications of Nanotechnology (UC CEIN), United States, [⊥]SLAC National Accelerator Laboratory, Menlo Park, California 94025, United States, [∥]European Synchrotron Radiation Facility, B.P.220-38043 Grenoble, Cedex, France, and [¶]Bren School of Environmental Science and Management, and Earth Research Institute, University of California, Santa Barbara, California 93106, United States

ABSTRACT With the increased use of engineered nanomaterials such as ZnO and CeO_2 nanoparticles (NPs), these materials will inevitably be released into the environment, with unknown consequences. In addition, the potential storage of these NPs or their biotransformed products in edible/reproductive organs of crop plants can cause them to enter into the food chain and the next plant generation. Few reports thus far have addressed the entire life cycle of plants grown in NP-contaminated soil. Soybean (*Glycine max*) seeds were germinated and grown to full maturity in organic farm soil amended with either ZnO NPs at 500 mg/kg or CeO_2 NPs at 1000 mg/kg. At harvest, synchrotron μ-XRF and μ-XANES analyses were performed on soybean tissues, including pods, to determine the forms of Ce and Zn in NP-treated plants. The X-ray absorption spectroscopy studies showed no presence of ZnO NPs within tissues. However, μ-XANES data showed O-bound Zn, in a form resembling Zn-citrate, which could be an important Zn complex in the soybean grains. On the other hand, the synchrotron μ-XANES results showed that Ce remained mostly as CeO_2 NPs within the plant. The data also showed that a small percentage of Ce(IV), the oxidation state of Ce in CeO_2 NPs, was biotransformed to Ce(III). To our knowledge, this is the first report on the presence of CeO_2 and Zn compounds in the reproductive/edible portion of the soybean plant grown in farm soil with CeO_2 and ZnO NPs.

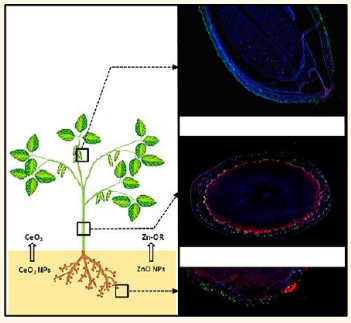

KEYWORDS: CeO_2 NPs · ZnO NPs · soybean · synchrotron · μ-XRF · TXM

The field of nanotechnology has increased so quickly that, by the year 2000, over 60 countries had established national programs on nanotechnology. One trillion dollars' worth of nanotechnology-based products are expected on the market by the year 2015.[1] Nanoparticles (NPs), one of the building blocks of nanotechnology, have a variety of applications due to their unique properties. Zinc oxide (ZnO) and cerium dioxide (CeO_2, nanoceria) NPs are among the most highly used NPs in industry.[2] ZnO NPs are widely used in sunscreen products, as gas sensors,[3] antibacterial agents,[4] optical and electrical devices,[5] and as pigments.[6] On the other hand, the high oxygen storage capacity of nanoceria makes it an excellent catalyst for internal combustion and oil cracking processes.[7,8] Nanoceria is also used for gas sensors,[9] sunscreen, and cosmetic creams.[10] However, after end-user applications, these products and residues will find their way into the environment, potentially reaching agricultural soils through biosolids.[11] Moreover, ZnO and CeO_2 NPs are potentially toxic to humans.[12,13]

The potential harmful effects of NPs taken up by crop plants have raised concerns in the scientific community and regulatory institutions; however, our knowledge about the impacts of NPs in the food chain is limited. Most of the nanotoxicological studies have been performed in a few crop plants in ideal conditions such as hydroponics and have included only the germination process and first growth stage of the

* Address correspondence to jgardea@utep.edu.

Received for review November 7, 2012 and accepted January 15, 2013.

Published online January 15, 2013
10.1021/nn305196q

plant.[14−16] As highlighted in a recent review,[17] our knowledge of plant nanotoxicology is in its infancy, and more studies are needed to fully understand the effects of NPs in plants. So far, few studies have documented the biotransformation of NPs in vegetative tissues within plants,[18−25] and there is a lack of information on the biotransformation of NPs in mature crops. To our knowledge, the first study of plants grown to maturity in NP impacted soil was only recently published in PNAS. In that study, Priester *et al.*[26] determined the effects of NP exposure on Ce and Zn accumulation and growth parameters of soybean (*Glycine max*) plants grown in farm soil with nanoceria and ZnO NPs.

Soybeans are the largest producers of edible oil and plant protein[27] and in 2010 were the fifth highest crop produced in the world and second in the USA.[28] Biotransformation of CeO_2 and ZnO NPs in hydroponically grown soybean seedlings has been studied with bulk X-ray absorption spectroscopy.[25] Synchrotron microfocused X-ray fluorescence (μ-XRF) and micro-X-ray absorption near-edge structure (μ-XANES) have been used to determine the speciation of arsenic in the rhizosphere of mesquite (*Prosopis juliflora-velutina*)[29] and the relationship between speciation and distribution of zinc in the Zn hyperaccumulator *Arabidopsis halleri*.[30] More recently, these techniques were used to study the chemical form and localization of titanium in cucumber (*Cucumis sativus*) plants treated with TiO_2 NPs[22] and the form of CeO_2 in roots of corn (*Zea mays*) seedlings.[31]

The present report describes, with the use of μ-XRF and μ-XANES, the forms of Ce and Zn within soybean tissues, including the reproductive organ, and analyzes the possible transfer of nanoceria and ZnO NPs into the food chain.

TABLE 1. Bioconcentration Factors (Metal in Tissue/Metal in Soil)

soil metal concentration	root	nodule	stem	pod	leaf
control 94.83 mg Zn/kg[a]	0.33	0.21	0.21	0.34	0.9
control 30.91 mg Ce/kg[a]	0.0095	0.0038	0.0013	0.0024	6×10^{-6}
500 mg of ZnO/kg	0.24	0.07	0.25	0.16	0.69
1000 mg of CeO_2/kg	0.21	0.011	0.0001	0.00004	3×10^{-7}

[a] Zn and Ce are naturally present in soil; therefore, the bioconcentration factors of the control were considered. Calculated from values reported in Priester *et al.*[26]

RESULTS AND DISCUSSION

ICP-OES and ICP-MS data from a previous study showed that soybean plants grown in organic farm soil spiked with ZnO or CeO_2 NPs take up and translocate Zn and Ce throughout the plant.[26] Table 1 shows that the bioconcentration factors (BCF) for Ce in the aerial plant parts were <0.001 (stems, leaves, and pods). Hence, the μ-XRF and μ-XANES analyses were focused on the nodules since these are part of the root system and involved in the nitrogen fixation process. In addition, we focused our spectroscopic studies on the soybean pod due to its importance in the food industry.

Figure 1A shows the Ce L(III) XANES spectra of Ce model compounds Ce acetate, Ce carbonate, CeO_2 NPs, Ce sulfate, and Ce hydroxide. We used these as reference compounds in order to perform linear combination fitting (LCF) analysis of the plant samples to determine speciation of Ce. Figure 2a shows an optical micrograph of the transverse section of a root nodule from a soybean plant grown in soil with CeO_2 NPs, while Figure 2b shows the μ-XRF Ce intensity map of the nodule. As shown in Figure 2b, Ce was mainly localized in the epidermis; however, Ce was also observed inside the nodule. Figure 2c shows the spectra

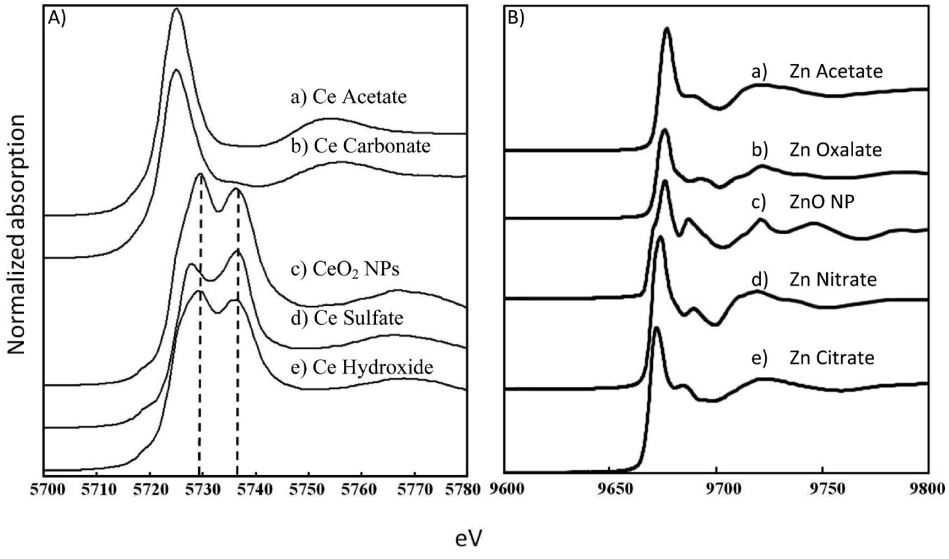

Figure 1. (A) Ce L(III) XANES of the Ce model compounds. Dotted lines at 5729 and 5737 eV illustrate the characteristic double white line in Ce(IV). (B) Zn K-edge XANES of the Zn model compounds.

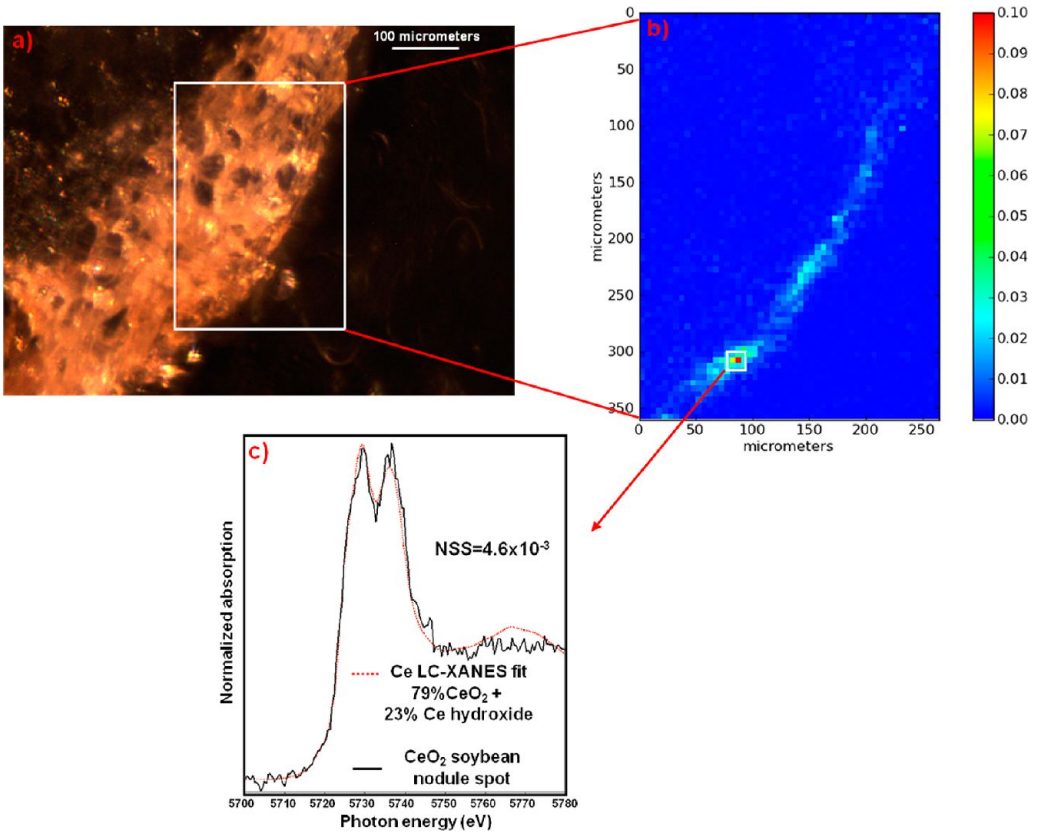

Figure 2. Images of the transversal section of a nodule from soybean plant grown in soil treated with 1000 mg of CeO_2/kg. (a) Video microscope image of the nodule section. (b) μ-XRF temperature map showing normalized Ce intensity; red represents higher Ce intensity, and dark blue represents the absence of a Ce signal. The white box area indicates where μ-XANES was acquired. (c) Ce L(III) μ-XANES from a high intensity Ce spot in the nodule (solid, black color) and the spectra from the linear combination fitting (dotted, red color). Normalized sum-squared residuals (NSS) are shown next to the fitting. $NSS = \Sigma_1(XANES_{experimental} - XANES_{fit})^2/\Sigma_1(XANES_{experimental})$.

from the high intensity Ce spots and the LCF. From the LCF, it was estimated that approximately 79% of the Ce was bound as CeO_2, maintaining the original CeO_2 NP coordination. This corroborates the scanning transmission electron microscopy and energy-dispersive spectroscopy (STEM EDS) results that showed particulate accumulations of Ce in the soybean nodules.[26] The tricolor μ-XRF map of the soybean pods (Figure 3a) shows low intensity Ce signal spots, which demonstrates that low amounts of Ce were translocated to the pod. This agrees with the low BCF obtained from the ICP-OES and ICP-MS results (Table 1). μ-XANES spectra were also acquired from a few selected spots within the area scanned in the μ-XRF Ce intensity map and tricolor map (Figure 3b,c, respectively). Figure 3d shows that the analyzed spectra from the μ-XRF Ce intensity map resemble the CeO_2 NP spectra, and the LCF data corroborate that 88% of the Ce in the analyzed spots were associated in the same way as the CeO_2 NP model compound. This suggests that most of the Ce was stored in the soybean pods as CeO_2 NPs. Previous bulk XANES analyses on alfalfa (*Medicago sativa*), corn, cucumber, and tomato (*Solanum lycopersicum*) seedling samples treated with CeO_2 NPs in hydroponics showed that CeO_2 NPs were the main chemical species of Ce within the plantlets.[14] Furthermore, Zhao *et al.*,[31] using μ-XRF and μ-XANES techniques, found that Ce was coordinated as CeO_2 NPs inside the roots of corn plants grown in organic soil amended with alginic acid coated CeO_2 NPs. Zhao *et al.*[31] also reported confocal microscopy images of fluorescein isothiocyanate-stained CeO_2 NPs in the cell walls of corn root cortex, suggesting passive uptake of the CeO_2 NPs.

In order to obtain further insights into the speciation of Ce in soybean plants, a peak fitting (PF) data analysis method was performed on the soybean pod and nodule high intensity Ce spots. The double white line marks at 5729 and 5737 eV present in the spectra from all of the analyzed spots (pod and nodule) show a signature, where Ce is mainly present in the Ce(IV) oxidation state (*e.g.*, compounds in Figure 1A). However, compared with the CeO_2 NP spectra (Figure 4b), the spectra from the Ce high intensity spots in the soybean pod show an increase in the amplitude (area) of peak C (Figure 4a). This can be attributed to an increased contribution of Ce(III) in the sample. The results suggest that internalization of CeO_2 within the soybean pod is affecting the structural order of Ce, which in turn can provide a surface susceptible for reduction. Similarly, Zhao *et al.* found that the

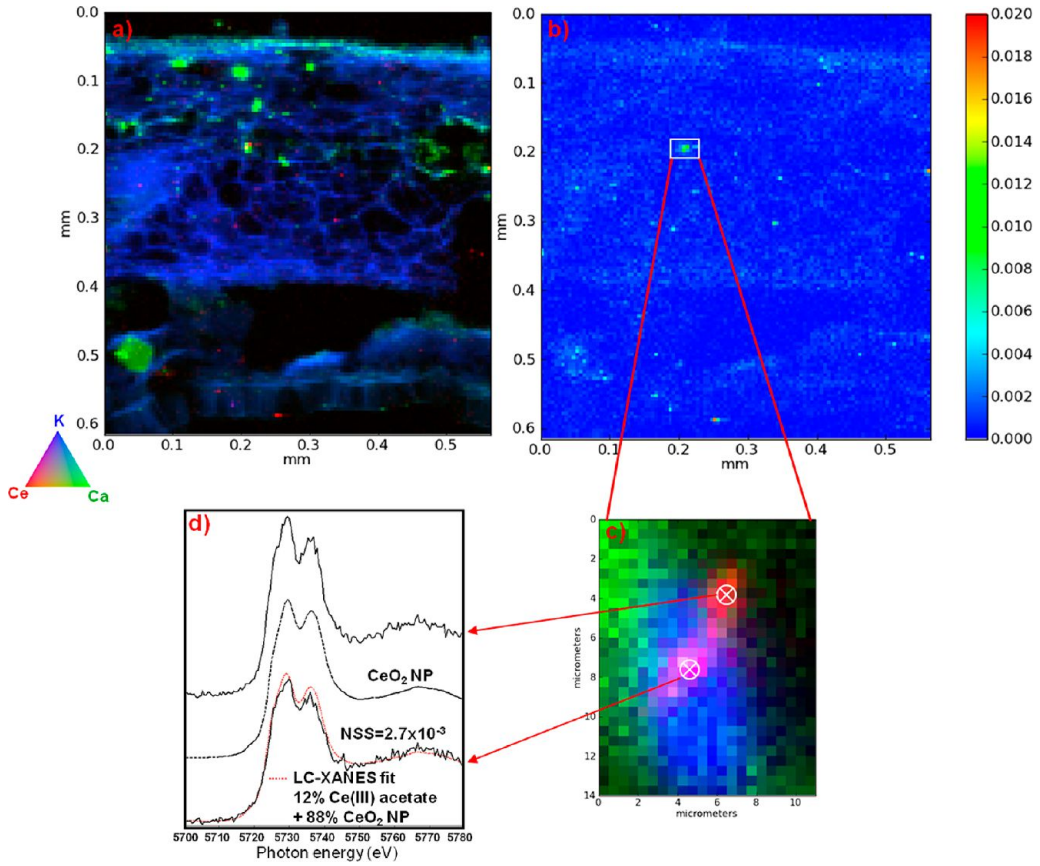

Figure 3. Images of the transversal section of a soybean pod grown in soil treated with 1000 mg of CeO_2/kg. (a) Tricolor μ-XRF map (red = Ce, green = Ca, blue = K). (b) μ-XRF temperature map of same location in (a) showing normalized Ce intensity. (c) Blowup of tricolor μ-XRF map from (b) (red = Ce, green = Ca, blue = K). White cross marks indicate where Ce L(III) μ-XANES were collected. (d) Ce L(III) μ-XANES spectra from selected spots, CeO_2 NP model compound, and the spectra from the linear combination fitting (dotted, red color). Normalized sum-squared residuals (NSS) are shown next to the fitting. NSS = $\Sigma_1(XANES_{experimental} - XANES_{fit})^2/\Sigma_1(XANES_{experimental})$.

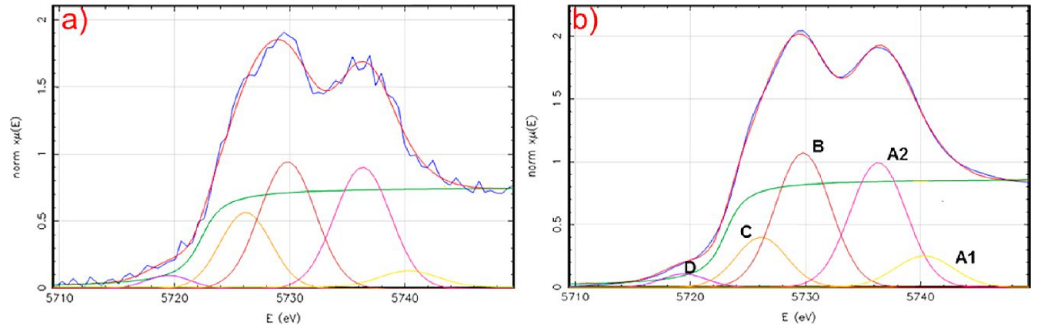

Figure 4. Peak fitting for (a) Ce L(III) μ-XANES from a high intensity Ce spot in the μ-XRF map in the pod. (b) CeO_2 NP model compound. A1 and A2 correspond to transitions to Ce d-orbitals with crystal field splitting of the $2p^4f^05d^*$ final state, and peak B represents transitions to a core-excited configuration $2p^4f^15d^*L$ (2p denotes the hole in the 2p shell, and 5d* refers to the excited electron in the 5d state; L stands for a hole in the anion ligand). C represents transitions to a combination of orbitals with crystal field splitting and excitation of different amounts of Ce(III) present in the samples. The pre-edge peak D is the result of a dipole-forbidden $2p^{3/2} \rightarrow 4f$ transition.

interaction of CeO_2 NPs with corn plant roots affected the oxidation state of Ce.[31] In the present work, a reduction in the intensity of the white line feature, compared with the CeO_2 NPs, was observed (Figure 4). Roggenbuck *et al.* reported a similar result in a comparison study of nanoporous CeO_2 and bulk CeO_2, attributed to a change in the surface-to-volume ratio.[32]

Figure 1B shows the XANES spectra of the Zn model compounds used for LCF. These model compounds included ZnO NPs, Zn-acetate, Zn-citrate, Zn-nitrate, and Zn-oxalate. These spectra were used to compare with spectra from ZnO NP-treated samples. Figure 5 shows tricolor maps obtained from the μ-XRF images of the nodule, stem, and pod. The BCF for Zn (Table 1)

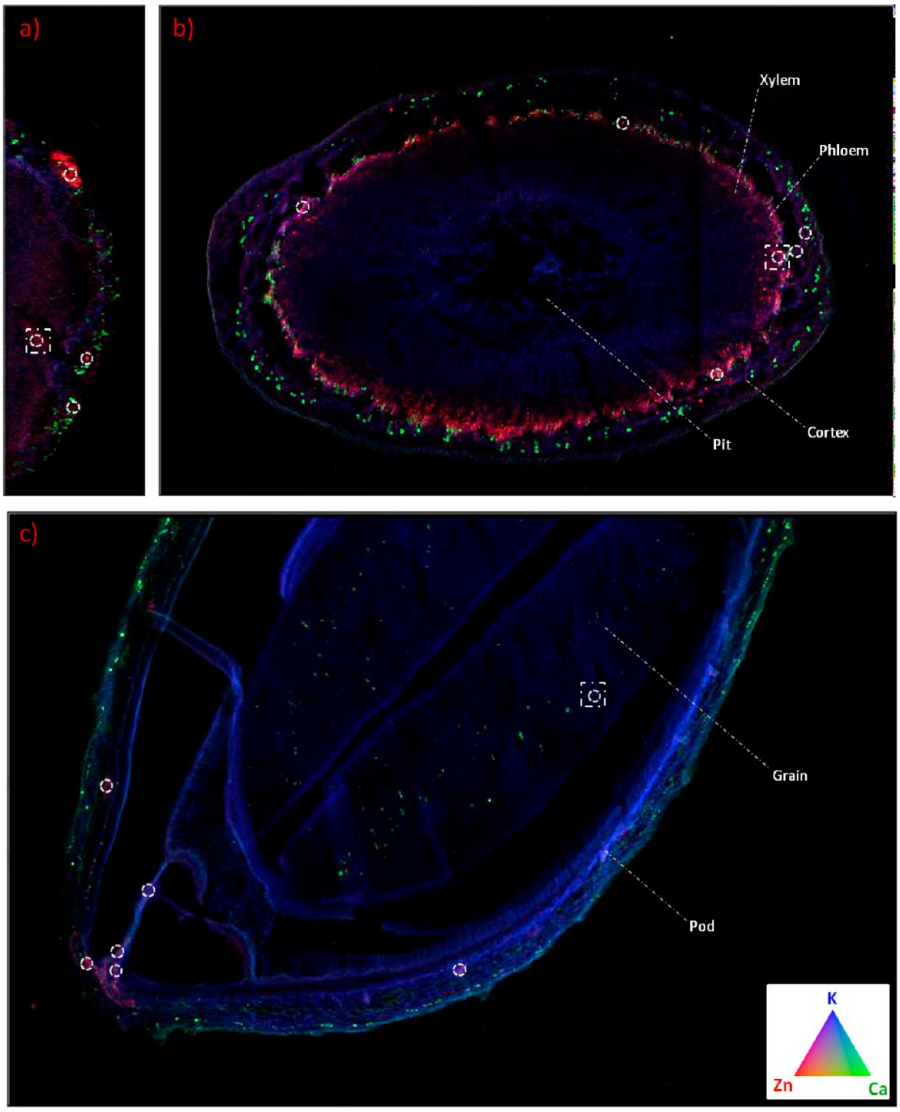

Figure 5. Tricolor μ-XRF maps (red = Zn, green = Ca, blue = K): (a) nodule, (b) stem, and (c) pod maps. μ-XANES was performed in areas of high Zn intensity marked by white circles. White square denotes the area from which spectra are shown in Figure 6.

in both the control and treated samples indicates that the soybean plants translocate Zn to the aerial portion of the plant. The highest concentration of Zn in the nodule was in the epidermis, where high Zn intensity spots can be observed (Figure 5a). The μ-XRF image from the soybean stem (Figure 5b) shows that most of the Zn was found in the phloem, which is part of the vascular system of the plant. Riesen and Feller[33] reported that, compared to other heavy metals, radiolabeled Zn was preferentially accumulated in the phloem of wheat plants (*Triticum aestivum* L. *cv.* "Arina"). As can be observed in the μ-XRF map (Figure 5c), we found high Zn intensity signals in the outer pod, although Zn was also present in the soybean grain. White marks in Figure 5 represent areas with high Zn intensity in the μ-XRF map. These areas were chosen in order to perform μ-XANES analysis. The results from all of the analyzed spectra (Figure 6) suggest that the Zn within the soybean plant was no longer in the form of ZnO NPs. We also performed synchrotron-based TXM studies on the soybean pod (Figure 7). From the Zn micro-XRF intensity map (Figure 7a), a high intensity section was chosen to perform TXM at 30 nm resolution. Dark precipitates are observed in Figure 7b,c; these dark structures were confirmed to be Zn by the μ-XANES Zn-edge signal (Figure 6d). The spectra from the Zn precipitate (Figure 6d) did not correctly fit any of our model compounds; however, they share a high level of resemblance with the Zn-citrate spectra (Figure 6e), indicating Zn–O ligation. Other researchers have suggested the possibility of Zn precipitation on cowpea root (*Vigna unguiculata*).[34] On the other hand, Figure 6 shows spectra taken from the μ-XRF tricolor maps (Figure 5, white squares). The spectra from the nodule (Figure 6c) had closest similarity to the Zn-citrate and Zn-nitrate, whereas the stem and pod spectra show a closest fit to Zn-citrate (Figure 6a,b). However, we are well aware that the accuracy of the LCF rests on the model compounds.

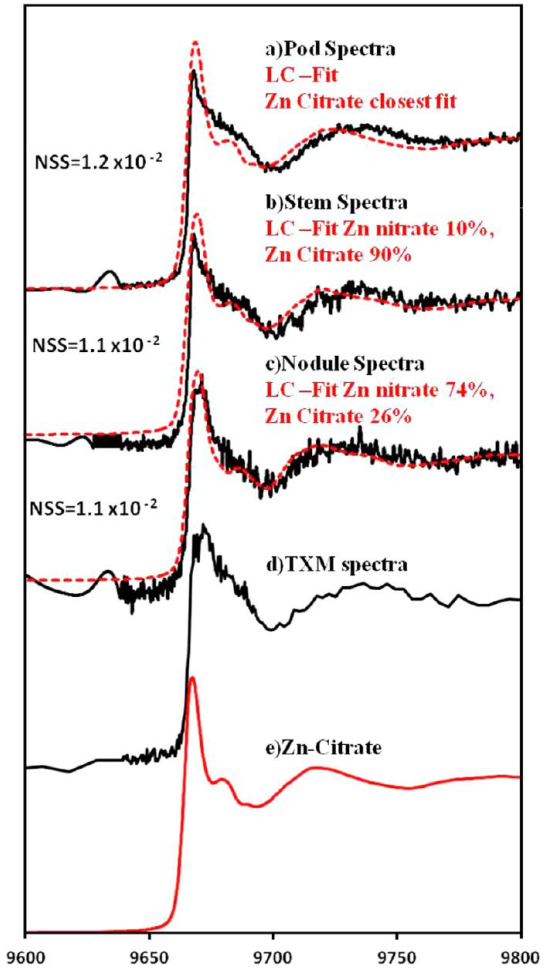

Figure 6. Zn K-edge XANES spectra from soybean samples grown with ZnO NPs in the soil. Linear combination fittings for (a) pod, (b) stem, and (c) nodule. Spectra with red dotted lines represent fits, and black solid line spectra represent μ-XANES from the sample. Normalized sum-squared residuals (NSS) are shown next to the fitting. (d) TXM spectra from the area indicated in (b. (e) Zn-citrate model compound.

Sarret and co-workers found that spectra of a mixture of organic acids (malate, citrate, and oxalate) and Zn-phosphate had a close fit with spectra from the hyperaccumulator plant *Arabidopsis halleri*.[30] We have observed similar results in previous studies of mesquite (*Prosopis juliflora-velutina*) exposed to ZnO NPs, where the μ-XANES spectra suggested a Zn–O ligand.[35] However, the study from Thangavel *et al.*[36] on cell suspension cultures of red spruce (*Picea rubens* Sarg.) suggests that, in living cells, it is likely that Zn ions bind to the sulfur of phytochelatins rather than to oxygen of organic acids. The ZnO NPs or their dissociated Zn ions could trigger the biosynthesis of phytochelatins, which are well-known indicators of heavy metal toxicity in plants. Nevertheless, all of the μ-XANES and linear combination data from high Zn intensity spots in the μ-XRF maps suggest that Zn(II) in the soybean plants was associated with oxygen because its spectra resemble the spectra of organic acids from the model compounds (Figure 6). LCF of bulk XANES of ground up plant tissues also indicated Zn ligation to O (data not shown). Lombi *et al.*[37] used a novel detector for complex natural samples (Maia detection system) to minimize radiation damage and dehydration of samples. By using the same detector, Kopittke and co-workers analyzed cowpea (*Vigna unguiculata*) exposed to Zn.[34] These investigators also found a Zn–O bond and determined that 65–85% of the Zn was bound as a Zn-phytate complex. Phytic acid is present in soybean plants and is the main form of phosphorus storage.[38] However, for this investigation, we did not have a Zn-phytate model compound. Nevertheless, by comparing the spectral shapes from Zn-phytate with the Zn in the soybean, we concluded they were not a good match.

CONCLUSIONS

Key issues in studying the interaction of crop plants with NPs are the determination of their entrance in the food chain, their biotransformation, and the possible presence of the NPs or their derived products in the next plant generation. The results of this study have shown that soybean plants grown in soil impregnated with ZnO NPs did not accumulate these NPs in the grains. The XANES data suggest that the Zn accumulated in the seeds of soybean plants is linked to O, resembling the form of Zn-citrate. To our knowledge, this is the first time that the translocation of Zn from ZnO NPs in soil grown soybean pods has been reported. On the other hand, although the BCF for Ce in soybean pods was low, the LCF results suggest that most of the Ce stored in the soybean pods was in the form of CeO_2 NPs. The PF results also suggest that a small percentage of the Ce in the pod could be changing its oxidation state from Ce(IV) to Ce(III). The results of these analyses have shown that CeO_2 NPs in soil can be taken up by food crops. This suggests that CeO_2 NPs can reach the food chain and the next soybean plant generation.

EXPERIMENTAL METHODS

Soybean Growth. As described by Priester *et al.*,[26] organic farm soil (OFS) (from Carpinteria, CA, N 34° 23′ 40″, W 119° 28′ 40″) was sieved (2 mm), air-dried, and stored at 4 °C. The OFS was spiked with either ZnO (10 nm) or CeO_2 (8 nm) NPs (Meliorum Technologies, Rochester, NY) at concentrations of 500 or 1000 mg kg^{-1}, respectively, 24 h prior to planting. The characterization of these NPs was previously reported by Keller *et al.*[39] Dwarf soybean seeds (variety, Early Hakucho, product #5555) were acquired from Park Seed Company (Greenwood, SC). The planting methodology is described elsewhere.[26] Briefly, nodulating bacteria (*Rhizobium japonicum* strain USDA 110) were added to the soybean seeds prior to the sowing. The seeds were planted in PVC trays for 4–7 days until cotyledons appeared. Later, the plantlets were transplanted to pots that contained 2400 g of soil. Four pots per treatment were

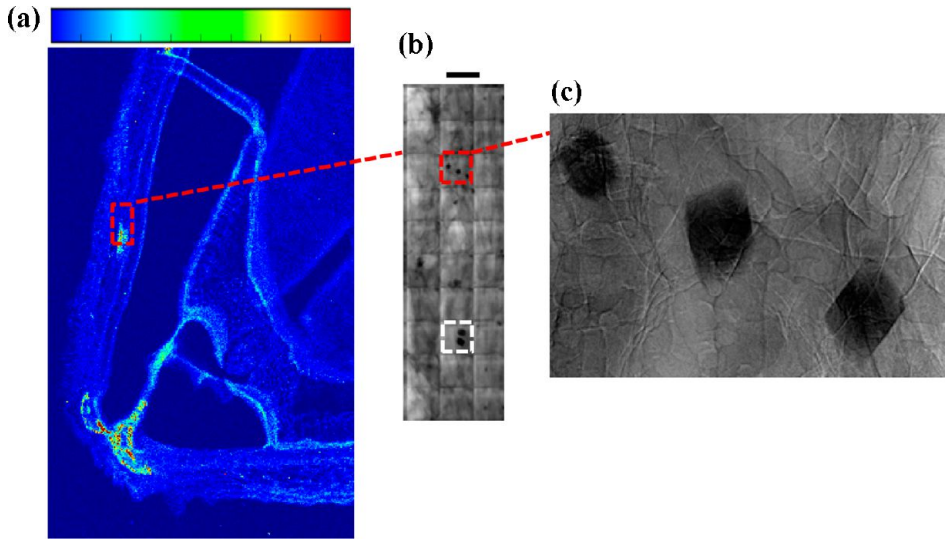

Figure 7. Images of the transversal section of a soybean pod grown in soil treated with 500 mg of ZnO/kg. (a) Zn μ-XRF map, where the red square denotes the area where TXM was performed. (b) TXM image, where the red square indicates a magnification of the area shown in (c). White square denotes the area where Zn K-edge μ-XANES were collected.

planted, while another four were left unplanted as controls. A climate-controlled greenhouse under full sunlight with nominal maximum temperature of 27 °C was used for this experiment. Every 72 h, the pots were watered with 100 mL of tap water for days 1−9. The volume of water changed with plant growth: the pots received 200, 250, and 300 mL for days 9−21, 21−27, and 27−48, respectively. The unplanted pots received an average of 100 mL/day watering for the duration of the experiment. The plants were harvested after 48 days of growth.

Sample Preparation. At harvest, roots of soybean plants treated with 500 mg/kg of ZnO NPs and 1000 mg/kg of CeO_2 NPs were washed twice with 0.01 M HNO_3 and three times with deionized (DI) water to eliminate any surface contaminants.[26] Soybean plants were cut with a scalpel into root, nodule, low stem, high stem, and pod before transferring them to liquid nitrogen for 30 min. The plant parts were embedded in Tissue Tek (Sakura Finetek USA, Torrance, CA) and axially sectioned (10 μm thick) with a cryomicrotome (Triangle Biomedical Sciences, Durham, NC) at −20 °C and mounted onto Kapton and Ultralene film. Sections were subsequently freeze-dried for 2 h in a Labconco freeze-dryer (FreeZone 4.5, Kansas City, MO) with operating conditions of −53 °C and 0.140 mBar pressure. For bulk XAS analysis, samples were flash frozen in liquid nitrogen and freeze-dried for 3 days. Afterward, dried tissues were ground to obtain a fine powder, loaded into aluminum sample holders, and covered with Kapton tape.

***μ*-XRF and *μ*-XANES Studies at ESRF.** μ-XRF mapping of the distribution of Ce and other elements in the soybean plant was performed with an incident energy of 5.8 KeV during 16-bunch mode at beamline ID21 of the European Synchrotron Radiation Facility (ESRF, Grenoble, France).[40] The storage ring current during data acquisition ranged between 60 and 90 mA operating at 6.0 GeV. The beam was focused with the use of K−B optics to 0.60 × 1.1 μm^2 ($V \times H$). The fluorescence signal was detected by a Si drift detector. Two photodiodes were used to measure the incident and transmitted beam intensities. Dwell time and distance of the detector were optimized for each image, keeping the detector dead time below 15%. The X-ray fluorescence data were processed using PyMCA software.[41] For μ-XANES data acquisition, the energy was selected using a Si(111) monochromator and scanned from 5.70 to 5.80 keV. The final Ce L(III) edge spectra were the sum of 5−60 individual scans with 0.1 s integration time and 0.5 eV step size. Each individual spectrum was inspected for beam induced changes, and the samples were stable in all cases. μ-XANES data analysis was carried out using Athena software.[42]

The linear combinations fit range was 5.700−5.780 and 9.600−9.800 keV for Ce and Zn samples, respectively. Normalized sum of square residuals were used as a measure of the discrepancy between the unknown data and the fit model.

For the PF data analysis, the pre-edge background was subtracted and normalized using a linear pre-edge. All peaks were identified by least-squares fitting of Gaussian profiles and one arctangent function.[43]

***μ*-XRF and *μ*-XANES Studies at SSRL.** Synchrotron experiments were conducted at SSRL beamline 2−3, which uses K−B optics to achieve an optimized beam with dimensions of 2 × 2 μm. μ-XRF mapping was performed with 0.5 × 0.5 μm^2 step size and 250 ms dwell time using a Si(111) monochromator for energy selection and Vortex (SII) detector for X-ray fluorescence detection. μ-XRF images and μ-XANES data were analyzed using the Micro Analysis Toolkit[44] and SixPACK.[45] The Zn foil calibration was set at 9.659 keV. The data processing included dead time correction, multiple sweep data inspection to deglitch individual scans, energy calibration, spectral averaging, background subtraction, principal component analysis, and linear combination fitting to reference spectra. Beamline 6−2 was used to collect transmission X-ray microscopy (TXM) images above the Zn K-edge (9.7 keV) with optics providing 30 nm resolution and 30 μm field of view. Multiple fields of view were acquired by raster scanning the sample. XANES were collected using a Vortex (SII) detector in fluorescence mode, with slits narrowed to create a 5 μm beam size. Beamline 7−3 was used to analyze the model compounds and bulk soybean samples exposed to ZnO NPs. The operating conditions in the storage ring were 3 GeV beam energy, an 80−100 mA beam current. Zn K-edge spectra were collected using a Canberra 29-element germanium detector and Si(220) ψ90 monochromator.

Conflict of Interest: The authors declare no competing financial interest.

Acknowledgment. This material is based upon work supported by the National Science Foundation and the Environmental Protection Agency under Cooperative Agreement Number DBI-0830117. Any opinions, findings, and conclusions or recommendations expressed in this material are those of the author(s) and do not necessarily reflect the views of the National Science Foundation or the Environmental Protection Agency. This work has not been subjected to EPA review, and no official endorsement should be inferred. Portions of this research were carried out at the Stanford Synchrotron Radiation Lightsource, a directorate of SLAC National Accelerator Laboratory and an Office of Science User Facility operated for the U.S. Department of Energy Office of Science by Stanford University. Ce X-ray spectromicroscopy experiments were performed on the ID21

beamline at the European Synchrotron Radiation Facility (ESRF), Grenoble, France. The authors also acknowledge USDA Grant No. 2011-38422-30835, and NSF Grant No. CHE-0840525. J.L.G.-T. acknowledges the Dudley family for the Endowed Research Professorship in Chemistry. J.A.H.-V. acknowledges the Consejo Nacional de Ciencia y Tecnologia of Mexico (CONACyT) for financial support (Grant 131996).

REFERENCES AND NOTES

1. Sargent, J. F. *Nanotechnology: A Policy Primer*; CRS Report for Congress, **2012**.
2. Kahru, A.; Dubourguier, H. C. From Ecotoxicology to Nanoecotoxicology. *Toxicology* **2010**, *269*, 105–119.
3. Xu, H.; Liu, X.; Cui, D.; Li, M.; Jiang, M. A. Novel Method for Improving the Performance of ZnO Gas Sensors. *Sens. Actuators, B* **2006**, *114*, 301–307.
4. Tam, K. H.; Djurisic, A. B.; Chan, C. M. N.; Xi, Y. Y.; Tse, C. W.; Leung, Y. H.; Chan, W. K.; Leung, F. C. C.; Au, D. W. T. Antibacterial Activity of ZnO Nanorods Prepared by a Hydrothermal Method. *Thin Solid Films* **2008**, *516*, 6167–6174.
5. Klingshirn, C. ZnO: Material, Physics and Applications. *Chem. Phys. Chem.* **2007**, *8*, 782–803.
6. Li, C.; Liang, Z.; Xiao, H.; Wu, Y.; Liu, Y. Synthesis of ZnO/Zn_2SiO_4/SiO_2 Composite Pigments with Enhanced Reflectance and Radiation-Stability under Low-Energy Proton Irradiation. *Mater. Lett.* **2010**, *64*, 1972–1974.
7. Garcia, T.; Solsona, B.; Taylor, S. H. Nano-Crystalline Ceria Catalysts for the Abatement of Polycyclic Aromatic Hydrocarbons. *Catal. Lett.* **2005**, *105*, 183–189.
8. Bozek, F.; Mares, J.; Bozek, M.; Huzlik, J. *Emission of Particulate Matter While Applying the Envirox TM Additive*, Proceedings of the 5th WSEAS International Conference on Waste Management, Water Pollution, Air Pollution, Indoor Climate, Iasi, Romania, July 1−3, 2011; pp 170−175.
9. Liao, L.; Mai, H. X.; Yuan, Q.; Lu, H. B.; Li, J. C.; Liu, C.; Yan, C. H.; Shen, Z. X.; Yu, T. Single CeO_2 Nanowire Gas Sensor Supported with Pt Nanocrystals: Gas Sensitivity, Surface Bond States, and Chemical Mechanism. *J. Phys. Chem. C* **2008**, *112*, 9061–9065.
10. Yabe, S.; Sato, T. Cerium Oxide for Sunscreen Cosmetics. *J. Solid State Chem.* **2003**, *171*, 7–11.
11. Currie, V. C.; Angle, J. S.; Hill, R. L. Biosolids Application to Soybeans and Effects on Input and Output of Nitrogen. *Agric., Ecosyst. Environ.* **2003**, *97*, 345–351.
12. Lee, S. H.; Lee, H. R.; Kim, Y. R.; Kim, M. K. Toxic Response of Zinc Oxide Nanoparticles in Human Epidermal Keratinocyte HaCaT Cells. *Toxicol. Environ. Health Sci.* **2012**, *4*, 14–18.
13. Moos, P. J.; Olszewski, K.; Honeggar, M.; Cassidy, P.; Leachman, S.; Woessner, D.; Cutler, N. S.; Veranth, J. M. Responses of Human Cells to ZnO Nanoparticles: A Gene Transcription Study. *Metallomics* **2011**, *3*, 1199–1211.
14. Lopez-Moreno, M. L.; de la Rosa, G.; Hernandez-Viezcas, J. A.; Peralta-Videa, J. R.; Gardea-Torresdey, J. L. X-ray Absorption Spectroscopy (XAS) Corroboration of the Uptake and Storage of CeO_2 Nanoparticles and Assessment of Their Differential Toxicity in Four Edible Plant Species. *J. Agric. Food Chem.* **2010**, *58*, 3689–3693.
15. Lee, W. M.; An, Y. J.; Yoon, H. S.; Kweon, H. S. Toxicity and Bioavailability of Copper Nanoparticles to the Terrestrial Plants Mungbean (*Phaseolus radiatus*) and Wheat (*Triticum aestivum*): Plant Agar Test for Water-Insoluble Nanoparticles. *Environ. Toxicol. Chem.* **2008**, *27*, 1915–1921.
16. de la Rosa, G.; Lopez-Moreno, M. L.; Hernandez-Viezcas, J. A.; Peralta-Videa, J. R.; Gardea-Torresdey, J. L. Toxicity and Biotransformation of ZnO Nanoparticles in the Desert Plants *Prosopis juliflora-velutina*, *Salsola tragus* and *Parkinsonia florida*. *Int. J. Nanotechnol.* **2011**, *8*, 492–506.
17. Rico, C.; Majumdar, S.; Duarte-Gardea, M.; Peralta-Videa, J. R.; Gardea-Torresdey, J. L. Interaction of Nanoparticles with Edible Plants and Their Possible Implications in the Food Chain. *J. Agric. Food Chem.* **2011**, *59*, 3485–3498.
18. Wang, Z.; Xie, X.; Zhao, J.; Liu, X.; Feng, W.; White, J. C.; Xing, B. Xylem- and Phloem-Based Transport of CuO Nanoparticles in Maize (*Zea mays* L.). *Environ. Sci. Technol.* **2012**, *46*, 4434–4441.
19. Zhang, P.; Ma, Y.; Zhang, Z.; He, X.; Guo, Z.; Tai, R.; Ding, Y.; Zhao, Y.; Chai, Z. Comparative Toxicity of Nanoparticulate/Bulk Yb_2O_3 and $YbCl_3$ to Cucumber (*Cucumis sativus*). *Environ. Sci. Technol.* **2012**, *46*, 1834–1841.
20. Wang, H.; Kou, X.; Pei, Z.; Xiao, J. Q.; Shan, Z.; Xing, B. Physiological Effects of Magnetite (Fe_3O_4) Nanoparticles on Perennial Ryegrass (*Lolium perenne* L.) and Pumpkin (*Cucurbita mixta*) Plants. *Nanotoxicology* **2011**, *5*, 30–42.
21. Parsons, G.; Lopez, M. L.; Gonzalez, C. M.; Peralta-Videa, J. R.; Gardea-Torresdey, J. L. Toxicity and Biotransformation of Uncoated and Coated Nickel Hydroxide Nanoparticles on Mesquite Plants. *Environ. Toxicol. Chem.* **2010**, *29*, 1146–1154.
22. Servin, A. D.; Castillo-Michel, H.; Hernandez-Viezcas, J. A.; Corral Diaz, B.; Peralta-Videa, J. R.; Gardea-Torresdey, J. L. Synchrotron Micro-XRF and Micro-XANES Confirmation of the Uptake Translocation of TiO_2 Nanoparticles in Cucumber (*Cucumis sativus*) Plants. *Environ. Sci. Technol.* **2012**, *46*, 7637–7643.
23. Zhang, P.; Ma, Y.; Zhang, Z.; He, X.; Zhang, J.; Guo, Z.; Tai, R.; Zhao, Y.; Chai, Z. Biotransformation of Ceria Nanoparticles in Cucumber Plants. *ACS Nano* **2012**, *6*, 9943–9950.
24. Larue, C.; Laurette, J.; Herlin-Boime, N.; Khodja, H.; Fayard, B.; Flank, A. M.; Brisset, F.; Carriere, M. Accumulation, Translocation and Impact of TiO_2 Nanoparticles in Wheat (*Triticum aestivum* spp.): Influence of Diameter and Crystal Phase. *Sci. Total Environ.* **2012**, *431*, 197–208.
25. Lopez-Moreno, M. L.; de la Rosa, G.; Hernandez-Viezcas, J. A.; Castillo-Michel, H.; Botez, C.; Peralta-Videa, J. R.; Gardea-Torresdey, J. L. Evidence of the Differential Biotransformation and Genotoxicity of ZnO and CeO_2 Nanoparticles on Soybean (*Glycine max*) Plants. *Environ. Sci. Technol.* **2010**, *44*, 7315–7320.
26. Priester, J. H.; Ge, Y.; Mielke, R.; Horst, A. M.; Cole Moritz, S.; Espinosa, K.; Gelb, J.; Walker, S. L.; Nisbet, R. M.; An, Y. J.; *et al.* Soybean Susceptibility to Manufactured Nanomaterials with Evidence for Food Quality and Soil Fertility Interruption. *Proc. Natl. Acad. Sci. U.S.A.* www.pnas.org/cgi/doi/10.1073/pnas.1205431109.
27. Economic Research Service, United States Department of Agriculture. *Briefing Room: Soybeans and Oil Crops. Background*, **2012**. Available at http://www.ers.usda.gov/topics/crops/soybeans-oil-crops.aspx. Accessed October 16, **2012**.
28. Food and Agriculture Organization of the United Nations. http://faostat.fao.org/site/339/default.aspx. Accessed October 16 2012.
29. Castillo-Michel, H.; Hernandez-Viezcas, J. A.; Servin, A. D.; Peralta-Videa, J. R.; Gardea-Torresdey, J. L. Arsenic Localization and Speciation in the Root-Soil Interface of the Desert Plant *Prosopis juliflora-velutina*. *Appl. Spectrosc.* **2012**, *6*, 719–727.
30. Serret, G.; Williams, G.; Isaure, M.-P.; Marcus, M. A.; Fakra, S. C.; Frerot, H.; Pairis, S.; Geoffroy, N.; Manceau, A.; Saumitou-Laprade, P. Zinc Distribution and Speciation in *Arabidopsis halleri* × *Arabidopsis lyrata* Progenies Presenting Various Zinc Accumulation Capacities. *New Phytol.* **2009**, *184*, 581–595.
31. Zhao, L.; Peralta-Videa, J. R.; Varela-Ramirez, A.; Castillo-Michel, H.; Li, C.; Zhang, J.; Aguilera, R.; Keller, A.; Gardea-Torresdey, J. L. Effect of Surface Coating and Organic Matter on the Uptake of CeO_2 NPs by Corn Plants Grown in Soil: Insight into the Uptake Mechanism. *J. Hazard. Mater.* **2012**, *225−226*, 131–138.
32. Roggenbuck, J.; Waitz, T.; Wagner, T.; Lotz, A.; Fröba, M.; Tiemann, M. Ce L^{III}-XANES Investigation of Nanoporous CeO_2. *HASYLAB-Jahresbericht HASYLAB/DESY*, Hamburg, **2007**, 461−462.
33. Riesen, O.; Feller, U. Redistribution of Nickel, Cobalt, Manganese, Zinc, and Cadmium *via* the Phloem in Young and Maturing Wheat. *J. Plant Nutr.* **2005**, *28*, 421–430.

34. Kopittke, P. M.; Menzies, N. W.; de Jonge, M. D.; McKenna, B. A.; Donner, E.; Webb, R. I.; Paterson, D. J.; Howard, D. L.; Ryan, C. G.; Glover, C. J.; *et al. In Situ* Distribution and Speciation of Toxic Copper, Nickel and Zinc in Hydrated Roots of Cowpea. *J. Plant Physiol.* **2011**, *156*, 663–673.
35. Hernandez-Viezcas, J. A.; Castillo-Michel, H.; Servin, A. D.; Peralta-Videa, J. R.; Gardea-Torresdey, J. L. Spectroscopic Verification of Zinc Absorption and Distribution in the Desert Plant *Prosopis juliflora-velutina* (velvet mesquite) Grown with ZnO Nanoparticles. *Chem. Eng. J.* **2011**, *170*, 346–352.
36. Thangavel, P.; Long, S.; Minocha, R. Changes in Phytochelatins and Their Biosynthetic Intermediates in Red Spruce (*Picea rubens* Sarg.) Cell Suspension Cultures under Cadmium and Zinc Stress. *Plant Cell, Tissue Organ Cult.* **2007**, *88*, 201–216.
37. Lombi, E.; de Jonge, M. D.; Donner, E.; Kopittke, P. M.; Howard, D. L.; Kirkham, R.; Ryan, C. G.; Paterson, D. Fast X-ray Fluorescence Microtomography of Hydrated Biological Samples. *PLoS One* **2011**, *6*, e20626.
38. Hurrell, R. F.; Juillerat, M. A.; Reddy, M. B.; Lynch, S. R.; Dassenko, S. A.; Cook, J. D. Soy Protein, Phytate, and Iron Absorption in Humans. *Am. J. Clin. Nutr.* **1992**, *56*, 573–578.
39. Keller, A. A.; Wang, H.; Zhou, D.; Lenihan, G. C.; Miller, C. R.; Ji, Z. Stability and Aggregation of Metal Oxide Nanoparticles in Natural Aqueous Matrices. *Environ. Sci. Technol.* **2010**, *44*, 1962–1967.
40. Susini, J.; Salomé, M.; Neuhaeusler, O.; Dhez, O.; Eichert, D.; Fayard, B.; Somogyi, A.; Bohic, S.; Bleuet, P.; Martinez-Criado, G.; *et al.* The X-ray Microscopy and Micro-Spectroscopy Facility at the ESRF. *Synchrotron Radiat. News* **2003**, *16*, 35–43.
41. Solé, V. A.; Papillon, E.; Cotte, M.; Walter, P.; Susini, J. A Multiplatform Code for the Analysis of Energy-Dispersive X-ray Fluorescence Spectra. *Spectrochim. Acta* **2007**, *62*, 63–68.
42. Ravel, B.; Newville, M. Athena, Artemis, Hephaestus: Data Analysis for X-ray Absorption Spectroscopy Using IFEFFIT. *J. Synchrotron Radiat.* **2005**, *12*, 537–541.
43. Nachimuthu, P.; Shih, W.; Liu, R.; Jang, L.; Chen, J. The Study of Nanocrystalline Cerium Oxide by X-ray Absorption Spectroscopy. *J. Solid State Chem.* **2000**, *149*, 408–413.
44. Webb, S. M. The MicroAnalysis Toolkit: X-ray Fluorescence Image Processing Software. *AIP Conf. Proc.* **2011**, *1365*, 19610.1063/1.3625338.
45. Webb, S. M. SixPACK: A Graphical User Interface for XAS Analysis Using IFEFFIT. *Phys. Scr.* **2005**, *T115*, 1011–1014.